Article:
Dong, X., Griffo, A., Hewitt, D. et al. (2020) Reduced-order thermal observer for power modules temperature estimation. IEEE Transactions on Industrial Electronics, 67 (12). pp. 10085-10094. ISSN: 0278-0046

https://doi.org/10.1109/TIE.2019.2959483

Reduced-Order Thermal Observer for Power Modules Temperature Estimation

Xiaojun Dong, Antonio Griffo, *Member, IEEE,* David Hewitt, Jiabin Wang *Senior Member, IEEE*

***Abstract*—In this paper, a reduced order thermal observer with disturbance estimation is applied for temperature monitoring in a power electronics module. Although accurate thermal models of power electronics assemblies are widely available, based e.g. on computational fluid dynamics (CFD) solvers, their computational complexity hinders the application in real-time temperature monitoring applications. This paper proposes a reduced order state space observer to provide a real-time estimation of temperature in power electronics modules. The observer is coupled with a disturbance estimator, to minimize the error caused by uncertainties in the model and unknown operating conditions.**

***Index Terms*— reduced-order observer, thermal, disturbance estimation, power modules.**

I. Introduction

ADVANCES in modern power electronics have resulted in fast paced expansion in the areas of generation, transmission, distribution, and end-user consumption of electrical power [1]. In these new systems, the reliability of the power electronics is a challenge [2-4], especially in applications with strong safety requirements (e.g. aerospace and automotive) or where continuous operation is required to avoid costly maintenance (e.g. renewable energy). These applications provide specific challenges concerning reliability due to the requirement that they operate continuously for long periods of time in harsh environment without user intervention [5]. The effects of operating temperature and temperature cycling on converter reliability are well documented [6-7]. Lifetime of components decreases exponentially with an increase in temperature [8-9]. It is also well known that thermo-mechanical failure modes in devices and packaging are accelerated by temperature cycling.

Health management and reliability constitute a fundamental part of the design and development cycle of electronic products [10-12]. To ensure reliability, the thermal management of power converters has become an essential part of the convertor design process [13-16]. This change has been further driven by the strong desire for higher power density [17-18], increased efficiency power electronics systems. Accurate knowledge of power device die temperature is critical to the implementation of control and health management algorithms which have been proposed to monitor and extend the lifetime of power modules under in-service conditions [19].

Temperature variation can also be reduced using dynamically controlled cooling [20-21]. To achieve this, a suitable model of the cooling system behaviour must be available. To perform this analysis, a range of design variables, such as inlet air temperature, velocity of the air flow, material composition of the power modules, and the geometry of the assembly, must be considered. Examples of methods used to perform thermal analysis in power electronics include computational fluid dynamics (CFD), compact thermal model, and empirical lumped element model. Of the methods above, CFD can be used to simulate conductive and convective heat transfer simultaneously, providing the most accurate and detailed temperature distribution of the power electronic system under consideration. The high fidelity nature of the model this technique results in it being the most computationally intense, making it unsuitable for applications such as dynamic control where real-time execution are required.

A vast literature has been published on real-time temperature estimation in power electronics devices. The simplest methods rely on open-loop estimations which predict the devices temperature based on loss and thermal models [22]. The accuracy of these models and the sensitivity to uncertainties in operating conditions, e.g. cooling and ambient temperature, or device parameters, might affect the accuracy of estimation. Closed-loop estimation methods using observers have been proposed to address some of these drawbacks. Examples of thermal observers which have been developed and analysed can be found in [23-25]. A full-order temperature observer for a 1D Cauer thermal network is proposed in [23] to provide an estimation of the junction temperatures, given the power dissipation and ambient temperature. A complex 3D thermal network in conjunction with two observers to estimate temperature at fast and slow timescale, respectively, is presented in [26]. Although very accurate, these methods rely on the direct measurement of device temperature used in the feedback loop, which might be impractical in most applications. Uncertainties due to unknown coolant flow rate and parameters might also be difficult to address. [27] describes a parameter-changing

Manuscript received June 27, 2019; revised Oct 25, 2019; accepted Nov 16, 2019. This work was supported by the European Commission Horizon 2020 – Mobility for Growth Program, under Grant 636170.

The authors are with the Department of Electronic and Electrical Engineering, The University of Sheffield, Sheffield, UK, (e-mail: A.Griffo@sheffield.ac.uk)

observer for the estimation of the coolant temperature.

In order to implement a full-order closed loop observer it is necessary to supply some form of feedback. Full-order observers use the measurements of some of the states of a dynamical system to reconstruct the other not directly measured states. In cases where it is not necessary to estimate all states, e.g. when some of them are directly measured, a reduced-order observer may be used. In this paper, the use of a reduced-order observer is proposed to estimate the temperature of the power devices assuming that the temperature in a nearby location on the module substrate is directly measured using a temperature sensor (thermistor).

The main contribution of this paper is to include a closed-loop compensating mechanism in the thermal observer to reduce the effects of uncertainties in parameters, errors in the estimation of power losses and/or due to unknown boundary conditions, e.g. coolant flow rate. This additional feedback mechanism, implemented in a reduced-order observer, uses the temperature measurement of the inlet air and of a thermistor mounted on the power module substrate.

The remainder of this paper seeks to propose a method of achieving improved temperature predictions and is structured in the following way: In Section II, the structure of the power module used as a test vehicle in this work is introduced. In Section III, the structure of the lumped parameter model, and a method of parameter estimation is introduced. In Section IV, closed loop reduced order observer is developed based in the estimated parameters. In Section V, the time-domain disturbance observer is developed which improves model accuracy in the presence of power dissipation/air flow/air temperature errors. Finally in Section VI experimental data is presented to demonstrate the operation of the developed models under both DC and AC conditions respectively.

I. POWER MODULE

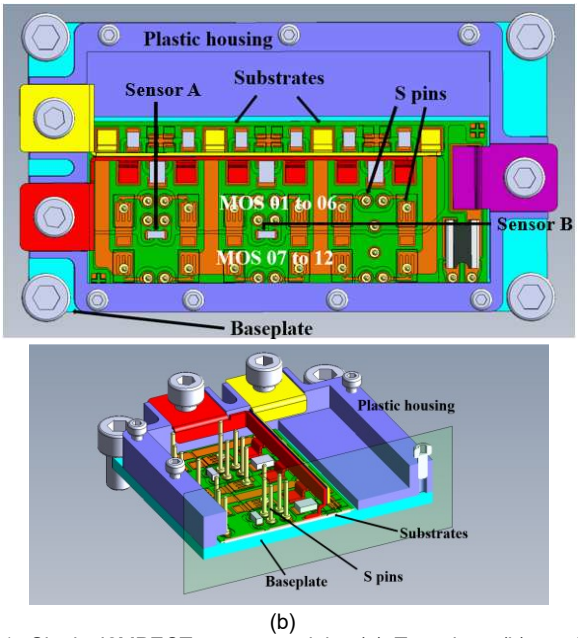

Fig 1. Single I2MPECT power module. (a) Top view; (b) cut iso view.

The power module used in this work is a Silicon Carbide (SiC) MOSFET-based half-bridge. Based on innovative wire-bond free planar interconnect technology [28-29], the module has been designed and manufactured by Siemens AG, within the Horizon2020 European Project - Integrated, Intelligent Modular Power Electronic Converter (I2MPECT)[30], to provide a power electronic building block (PEBB) for a 99% efficient 3-phase power converter with a power-to-weight ratio of 10 kW/kg. Fig 1 shows CAD drawings of the half-bridge wirebond-less power module. Twelve MOSFETs are sintered using a silver sintering paste onto the direct copper bonded (DBC) substrate. Two thermistors (PT1000), indicated as Sensors A, B in Fig. 1, are mounted on the DBC for temperature feedback. The module is primarily cooled via the baseplate, which is designed to be mounted to an air cooled heatsink via a thermal interface material.

II. THERMAL MODELLING

A thermal model of the power module and heatsink is established based on a Foster-type resistor-capacitor (RC) network as shown in Fig. 2. A coupled electro-thermal model is used to evaluate the losses in realistic operating conditions for the converter. This simplified RC compact thermal model is capable of taking into account lateral heat dissipation within the module and thermal interference between MOSFETs and the embedded PT1000 thermistor used as temperature sensor on the module baseplate. As shown in Fig. 2, the MOSFET losses are dissipated to the ambient via a third-order Foster network (R_1C_1 to R_3C_3). The temperature Sensor 'B' is thermally connected to the ambient via a first-order foster network (R_4C_4). The resistance R_{jB}, represents the thermal conduction between the device and temperature sensor. Therefore, the thermal network is of fourth order, making it relatively simple from a computational viewpoint and suitable for real-time application in a temperature monitoring system. The device junction temperature $T_j = X_1 + X_2 + X_3 + T_{air}$, where $X_{1,2,3}$ are the temperature rises across the respective RC elements. The lumped network could be replicated for each of the devices in the power module. For simplicity, in the following, only one network will be used to represent only the hottest device (MOS11). Power losses can be calculated using standard methods for the estimation of conduction and switching losses in PWM inverters [31] using temperature-dependent device characteristics [32]. The R_i, C_i parameters have been estimated using a parameters identification procedure based on CFD analyses. In particular, the model of a complete three-phase converter has been established in ANSYS Icepak CFD tool as shown in Fig 3. The three power modules are mounted on a forced air-cooled parallel plate finned heatsink and the transient response to a step increase in power dissipation, is calculated. The inlet air temperature of the ANSYS Icepak model is 40℃ with a fixed air flow rate of 4m/s. The three power modules are mounted on a forced air-cooled parallel plate finned heatsink and the transient response to a step increase of 450W in power dissipation, equally distributed across the 3×12 devices is calculated, as shown in Fig. 4. The results of this parameters extraction method are also shown in Fig. 4 demonstrating a good agreement between the CFD reference and the lumped parameter network. The

parameters resulting from the identification procedure are listed in the Appendix.

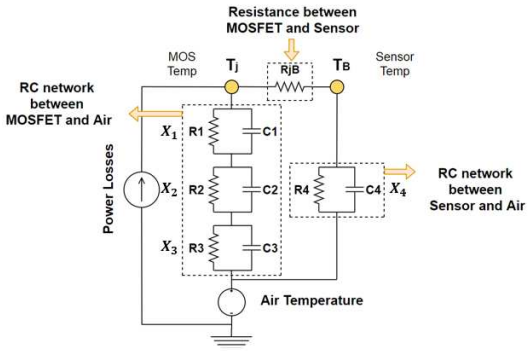

Fig 2. Lumped parameter thermal network.

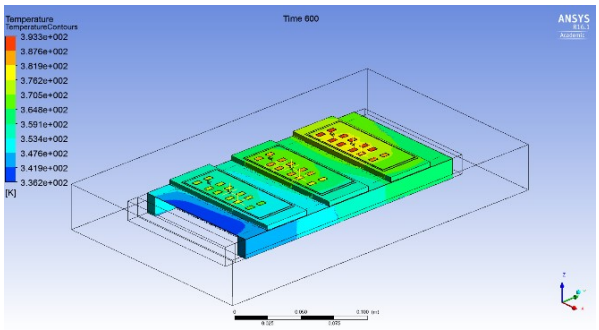

Fig 3. Model Simulation using ANSYS Icepak

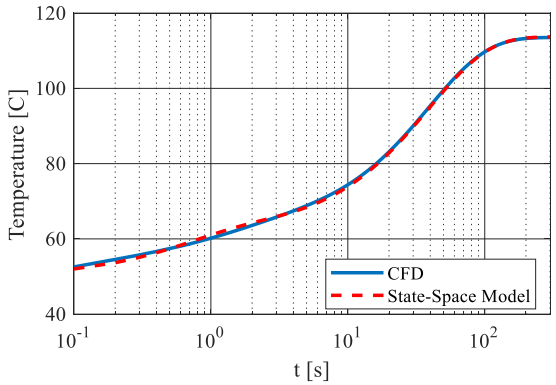

Fig 4. Transient thermal response for model parameter estimation

Using the derivation in the Appendix, the thermal model can be written in the state-space form as:

$$\dot{x} = Ax + Bu$$
$$y = Cx \qquad (1)$$

where x is the vector of states, y is the state outputs (T_j and T_B), u is the vector of inputs, A is the state matrix, B is the input matrix and C is the observation matrix, given by:

$$A = \begin{bmatrix} A_{11} & A_{12} \\ A_{21} & A_{22} \end{bmatrix} \qquad B = \begin{bmatrix} B_1 \\ B_2 \end{bmatrix}$$
$$C = \begin{bmatrix} 1 & 1 & 1 & 0 \\ 0 & 0 & 0 & 1 \end{bmatrix} \qquad u = \begin{bmatrix} P_{loss} \\ T_{air} \end{bmatrix}$$
$$x = \begin{bmatrix} x_1 \\ x_2 \\ x_3 \\ \dots \\ x_4 \end{bmatrix} = \begin{bmatrix} x_{MOS} \\ \cdots \\ x_{Sensor} \end{bmatrix} \qquad y = \begin{bmatrix} T_j \\ T_B \end{bmatrix} \qquad (2)$$

where:

$$A_{11} = \begin{bmatrix} -\frac{1}{C_1}\left(\frac{1}{R_1}+\frac{1}{R_{jB}}\right) & -\frac{1}{C_1 R_{jB}} & -\frac{1}{C_1 R_{jB}} \\ -\frac{1}{C_2 R_{jB}} & -\frac{1}{C_2}\left(\frac{1}{R_2}+\frac{1}{R_{jB}}\right) & -\frac{1}{C_2 R_{jB}} \\ -\frac{1}{C_3 R_{jB}} & -\frac{1}{C_3 R_{jB}} & -\frac{1}{C_3}\left(\frac{1}{R_3}+\frac{1}{R_{jB}}\right) \end{bmatrix}$$

$$A_{21} = \begin{bmatrix} \frac{1}{C_4 R_{jB}} & \frac{1}{C_4 R_{jB}} & \frac{1}{C_4 R_{jB}} \end{bmatrix}$$

$$A_{12} = [\frac{1}{C_1 R_{jB}} \quad \frac{1}{C_2 R_{jB}} \quad \frac{1}{C_3 R_{jB}}]^T \qquad A_{22} = \left[-\frac{1}{C_4}\left(\frac{1}{R_4}+\frac{1}{R_{jB}}\right)\right]$$

$$B_1 = \begin{bmatrix} \frac{1}{C_1} & 0 \\ \frac{1}{C_2} & 0 \\ \frac{1}{C_3} & \frac{1}{C_3}\left(\frac{1}{R_3}+\frac{1}{R_{jB}}\right) \end{bmatrix} \qquad B_2 = \begin{bmatrix} 0 & \frac{1}{C_4}\left(\frac{1}{R_4}+\frac{1}{R_{jB}}\right) \end{bmatrix}$$

III. Reduced Order Observer of Thermal Model

The model (1) could be used as an open-loop estimator of device temperature if the inputs, i.e. ambient temperature and power losses, and the parameters of the network are accurately estimated. This accurate knowledge of environmental conditions and parameters is rarely possible in practical applications. The paper proposes the use of an observer which provides a correction feedback mechanism which tries to correct the errors due to imprecise knowledge of conditions, inputs and parameters, e.g. caused by changes in the inlet air temperature and airflow rate and modelling errors e.g. in the estimated power loss and estimated thermal parameters.

A full-order observer, based on the thermal model discussed in Section II, can be written in state-space form as:

$$\dot{\hat{x}}(t) = A\hat{x}(t) + Bu(t) + L(y(t) - \hat{y}(t))$$
$$\hat{y}(t) = C\hat{x}(t) \qquad (3)$$

Where $\hat{x}(t)$ is the estimated state of the system, $\hat{y}(t)$ is observer output (estimated MOS junction temperature and estimated sensor temperature) and L is the gain of observer.

An observer is a dynamic system, designed to be an approximate replica of the real system, used to estimate the states of the real system. The observer is driven by the same inputs (MOS power loss and inlet air/ambient temperature) as the real system, with an additional correction term that is derived from the difference between the actual measurement y from the real system and predicted output $\hat{y}$ derived from the observer [23]. The correction term is composed of the error $y - \hat{y}$ and feedback matrix or gain. Consequently, an observer uses the difference between the measurement and prediction to improve prediction accuracy.

Due to the fact that there are no temperature sensors on the MOS chip, the state temperature cannot be measured directly. However, the module does incorporate two PT1000 thermistors used as temperature sensors attached to the DBC substrate. Therefore, the temperature of this sensor can be directly measured and does not need to be estimated. In this case, a reduced-order observer will suffice [33-34]. For the

thermal model analysed in the paper, the full system has 4 states $(X_1, \dots, X_4)$ however, one of them (X_4) can be measured directly as it represents the sensor temperature, therefore a reduced order observer with only 3 states is necessary. The derivation of the reduced-order observers is obtained by partitioning the state vector into two sub-states:

$$x = \begin{bmatrix} x_{MOS} \\ \cdots \\ x_{Sensor} \end{bmatrix}$$

$$x_{Sensor} = y = Cx = \hat{x}_{sensor} \tag{4}$$

Where $C = [0 \quad I]$ is the observation vector (of dimension m=1) and x_{MOS} (of dimension 3) comprises the component of the state vector that cannot be measured directly. The assumption that $y = x_{Sensor}$ makes the resulting equations simpler, but it is not necessary. Equivalent results can be obtained for any observation matrix C of rank m. In terms of x_{MOS} and x_{Sensor} the plant dynamics [33-34] are written as:

$$\dot{x}_{MOS} = A_{11}x_{MOS} + A_{12}x_{Sensor} + B_1 u$$

$$\dot{x}_{Sensor} = A_{21}x_{MOS} + A_{22}x_{Sensor} + B_2 u \tag{5}$$

$$\hat{x}_{sensor} = x_{Sensor} = y \tag{6}$$

For the remaining sub-states, we define the reduced-order observer by:

$$\hat{x}_{MOS} = Ky + z \tag{7}$$

Where z is the state of a system of order $m = 3$:

$$\dot{z} = \hat{A}z + Ly + Hu \tag{8}$$

A block-diagram representation of the reduced-order observer [33] is shown in Fig 5.

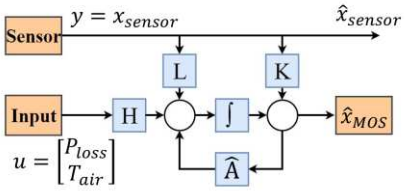

Fig 5. Reduced-order observer

It is necessary to ensure the convergence of the temperature estimation error $e_{MOS} = x_{MOS} - \hat{x}_{MOS}$ to zero. From the above equations:

$$\dot{e}_{MOS} = \hat{A}e_{MOS} + \left(A_{11} - KA_{21} - \hat{A}\right)x_{MOS} + \begin{pmatrix} A_{12} - KA_{22} \\ -L + \hat{A}K \end{pmatrix} x_{Sensor} + (B_1 - KB_2 - H)u \tag{9}$$

A sufficient condition for the error to converge to zero is to choose the matrices to satisfy [33-34]:

$$\hat{A} = A_{11} - KA_{21}$$

$$L = A_{12} - KA_{22} + \hat{A}K$$

$$H = B_1 - KB_2 \tag{10}$$

When the conditions shown in (10) are all satisfied, the error in estimation of x_{MOS} is given by

$$\dot{e}_{MOS} = \hat{A}e_{MOS} \tag{11}$$

Therefore the gain matrix K should be chosen to make the eigenvalues of $\hat{A} = A_{11} - KA_{21}$ lie in the open left-half plane. Additionally, A_{11} and A_{21} in the reduced-order observer take the roles of A and C in the full-order observer; once the gain matrix K is chosen, there is no further freedom in the choice of L and H.

IV. TIME-DOMAIN DISTURBANCE ESTIMATION

Device junction temperature depends not only on power dissipation but also on environmental conditions such as changes in ambient temperature, e.g. caused by heating of nearby devices mounted on the same cooling system, or changes in coolant flow rate. Changes in inlet air temperature and air flow will introduce an error between the estimated and real MOSFET temperature. To reduce estimation errors between the real value and reference values, a state observer may be used. Power losses are assumed to be subject to an estimation error, a disturbance estimation will be introduced to estimate and compensate this error. The so-called unknown input observer (UIO) have been evaluated in [34-37]. In this case, a typical state space model used for the UIO is

$$\dot{x} = Ax + Bu + B_d d$$
$$y = Cx \tag{12}$$

where x is the vector of states, y is the vector of measures (T_B), u is the vector of known inputs, representing the monitored air temperature, d is the vector of unknown inputs, representing the power loss estimation. A is the state matrix, B is the input matrix, C is the observation matrix and B_d is the unknown input matrix. Consequently, an UIO design is investigated for a linear system in (12). The general expression of the UIO [36] is

$$\dot{z} = -NB_d(z + Nx) - N(Ax + Bu)$$
$$\hat{d} = z + Nx \tag{13}$$

Where $B_d = \left[\frac{1}{C_1} \quad \frac{1}{C_2} \quad \frac{1}{C_3} \quad 0\right]^T$ and N the observer gain matrix need be designed. Consequently, the estimation error is

$$e = \hat{d} - d \tag{14}$$

And error dynamic is

$$\dot{e} = \dot{z} + N\dot{x} - \dot{d}$$
$$= -NB_d\hat{d} - N(Ax + Bu) + N(Ax + Bu + B_d d) - \dot{d}$$
$$= -NB_d\left(\hat{d} - d\right) - \dot{d} = -NB_d e - \dot{d} \tag{15}$$

Where $\dot{d}$ is zero in this model and the error dynamic equation can be rewritten as

$$\dot{e} = -NB_d e \tag{16}$$

It is shown that the disturbance estimation error system is stable if the observer gain matrix is chosen to make $-NB_d$ stable, i.e. a matrix whose eigenvalues have strictly negative real part [38-40]. When the disturbance estimation error system reaches steady state, $\dot{e}$ equals to zero and consequently, e equals to zero.

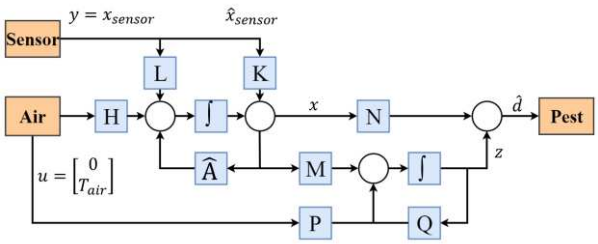

Fig 6. Thermal model with UIO disturbance estimation

The concept of disturbance estimation is illustrated in the block diagram of Fig 6. Based on equation (13), the relative parametric matrices are:

$$M = -NB_d M - NA$$
$$P = -NB$$
$$Q = -NB_d \qquad (17)$$

It is assumed that the input power loss is unknown and therefore can be assumed to be equal to the output of the disturbance estimation P_{est}. The air inlet temperature at the input duct of the heatsink is measured and fed as an input to the observer in Fig 6. The estimated loss P_{est}, at the output of the disturbance estimation in Fig. 6 is fed back as an input to the reduced-order observer in Fig. 5.

I. Experimental Validation

Fig 7 shows the experimental setup used to evaluate the discussed models. In this configuration, two resistors were used in place of power modules to simplify the construction. Both the resistors and power module are connected to DC power supplies. Both the two resistors and the power module are mounted to the heatsink via thermal pad (Kerafol KERATHERM Thermal Pad 6.5W/mK Gap Fill) to ensure good heat transfer.

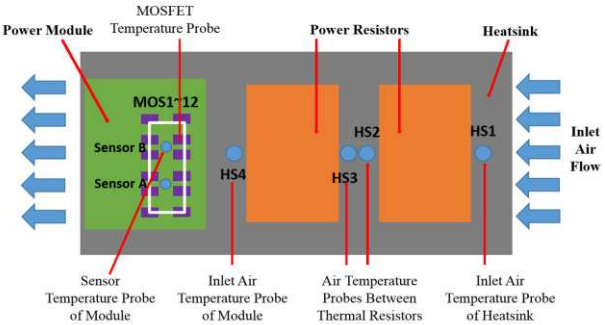

(a)

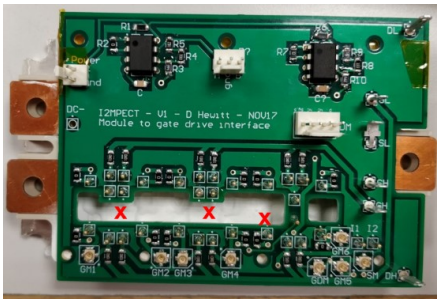

(b)

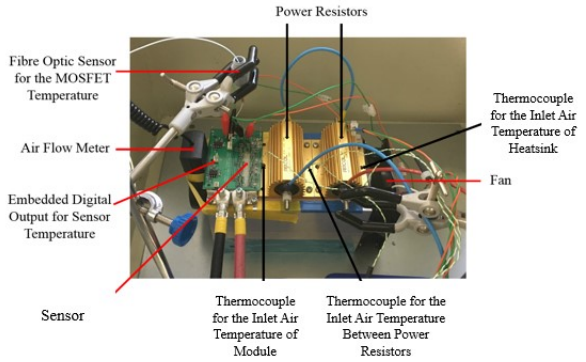

(c)

Fig 7. Experimental layout. (a) Thermal model design; (b) Figure of power module and gate drive board; (c) General view of experimental rig

As shown in Fig 7(a), the rig includes four thermocouples, positioned in the airflow at the inlet, outlet and in between the modules, allowing the air temperature to be monitored, although only the inlet air temperature measured by HS1 is used in the proposed observer.

The two embedded temperature sensors within the module are also monitored, one of which is the input variable of the reduced order observer in Section II. Additionally, a Fibre Optic temperature measurement system (Opsens Coresens GSX-2-N module and an OTF-F temperature sensor) is used to monitor MOSFET die temperature directly for comparison with the observer model predictions and validation of the proposed methodology [41]. As shown in Fig. 7b, the gate driver adapter board mounted on the power module features a cutout that allows direct visual and physical access to the three of the twelve MOSFETs in the module. The top surface of the module is coated with Boron-Nitride paint to provide a high emissivity surface for the thermal camera [42].

The heatsink used in these experiments is a typical hollow-fin heatsink (Fischerelectronik) with an integrated axial fan, as shown in the following Fig 8.

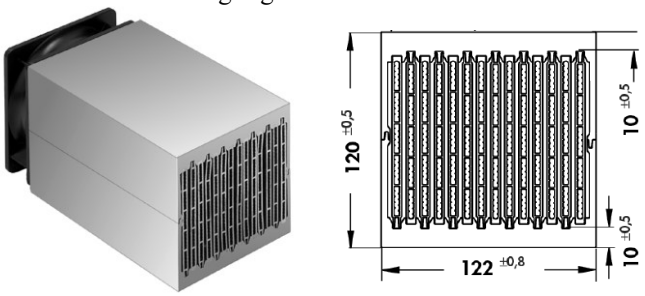

(a) (b)

Fig 8. Hollow-fin cooling aggregates. (a) The prototype of heatsink; (b) Cross-section layout of heatsink

Fig 9 illustrates the influence of airflow on the test platform. Here the same peak current of 70A is supplied in all cases. The convective boundary condition is affected by the air flow rate. Based on the same input power and experiment layout, the steady state temperature captured by thermal camera shows the effect of the change of the air flow rate on convective boundary condition. With an increasing air flow rate from 1m/s to 1.5m/s, the maximum temperature of the power module in steady state reduces from 103℃ to 94.1℃.

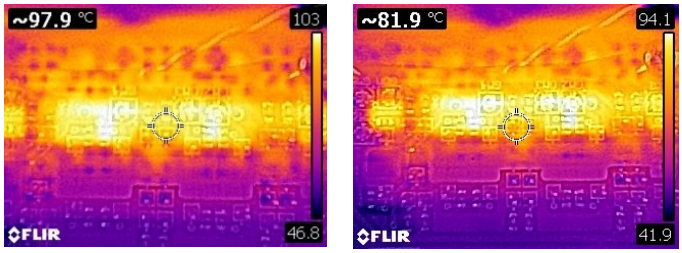

(a) (b)

Fig 9. Steady-State temperature from thermal camera. (a)1m/s for peak current of 70A; (b)1.5m/s for peak current of 70A;

Transient results obtained by testing at different current levels are shown in Fig 10. Using the measured inlet ambient temperature, the observer model with disturbance estimation can accurately predict the MOSFET temperature when compared with experimental data under different boundary conditions. This is despite the fact that the model parameters obtained in Section III are used (which were derived for the same module in a different experimental configuration).

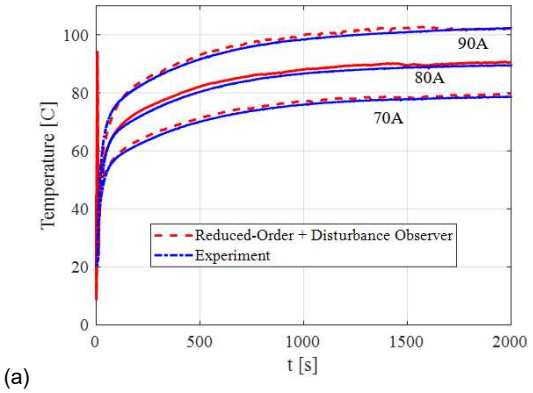

(a)

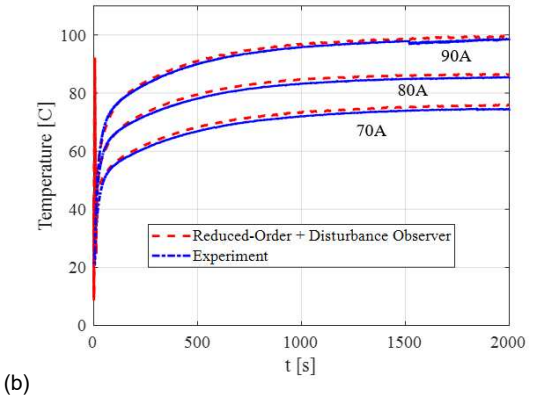

(b)

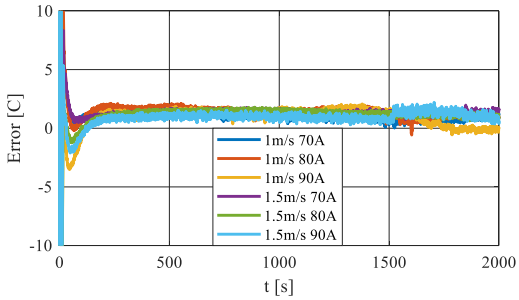

(c)

Fig 10. Comparison between experimental data and estimated values. (a) 1m/s for peak current of 70A, 80A and 90A ;(b) 1.5 m/s for peak current of 70A, 80A and 90A; (c) Transient error.

A more complex boundary condition is introduced to test the accuracy of the observer. In this test the air flow velocity is varied between three different values, furthermore, the DC current is also varied between three levels from 70A to 90A following the profile shown in Fig 11.

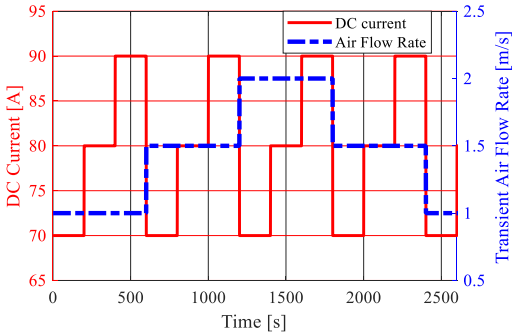

Fig 11. Experimental condition with variable DC current and air flow rate.

In Fig 12(a), excellent data agreement can be found in the validating process of reduced-order observer model against experiment in the complex condition with time-varying values of power loss and air cooling system, confirming the speed and accuracy of real-time monitoring as well we health management of power modules. A comparison between estimated power loss P_{est} and measured module power per chip is shown in Fig 12(b).

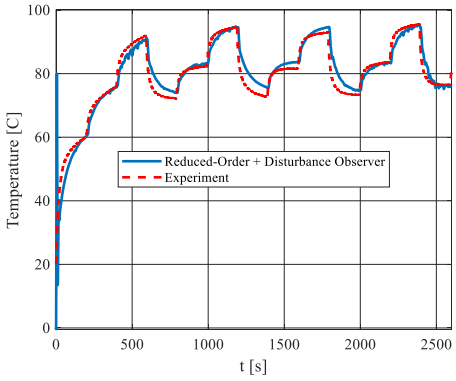

(a)

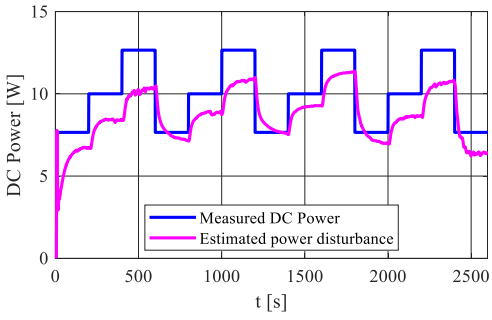

(b)

Fig 12. Comparison between experimental data and estimated values with time-varied DC current and transient air flow rate. (a) Comparison between estimated and measured MOSFET junction temperature; (b) Comparison between estimated power disturbance and measured module power per chip.

It is worth noting that the disturbance observer provides a feedback mechanism to compensate the effects of all the errors combined, e.g. due to uncertain loss estimation, ambient conditions and/or parameters. However, the observer cannot

provide an accurate separation of the multiple sources of errors and therefore cannot provide an estimation of the losses only. In the first validation, DC currents are used as source of power losses. These can be easily measured, reducing the uncertainties. The second experimental validation, provides a more challenging application of the proposed method including a relatively complex three-phase converter setup which is fully representative of real industrial applications. An alternative experiment layout is shown in Fig 13(a). The physical assembly of this configuration is shown in Fig 13(b) and Fig 13(c). This configuration includes three power modules. The module being monitored is mounted in the final positon on the heatsink (with respect to the airflow direction). The three power modules are driven to generate a three-phase AC output current into a three-phase resistive inductive (RL) load with a frequency of 200Hz. This configuration also differs from the previous tests in the manner in which the cooling system was constructed. In this new configuration, each module is mounted to an individual heatsink with ducting being used to enclose these heatsinks and direct the cooling air, with airflow being generated by the fan.

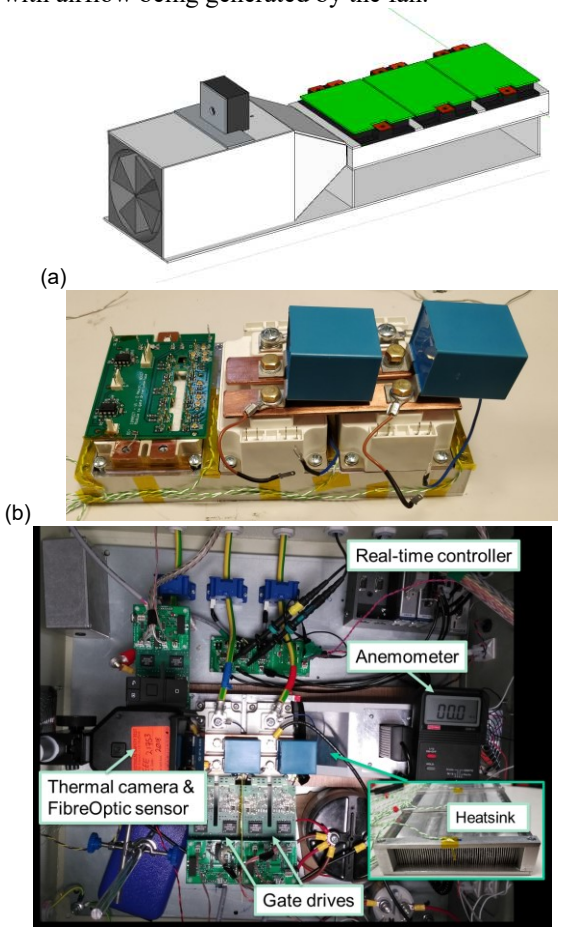

Fig 13. Diagrams of experimental setup: (a) Diagram of Channel/ducting final layout in experiment; (b) Mounting of modules on heatsink; (c) Full experimental test rig with three phase inverter

The data from the analytical model and experiment (shown in Fig 14) were compared to test the behaviour of the disturbance estimation observer. The experiment was repeated for a range of different peak current ranging from 50A to 90A, allowing the model to be evaluated for a range of different power losses. The input power losses in the analytical model is set to 0 to avoid the disturbance caused by power loss estimation error.

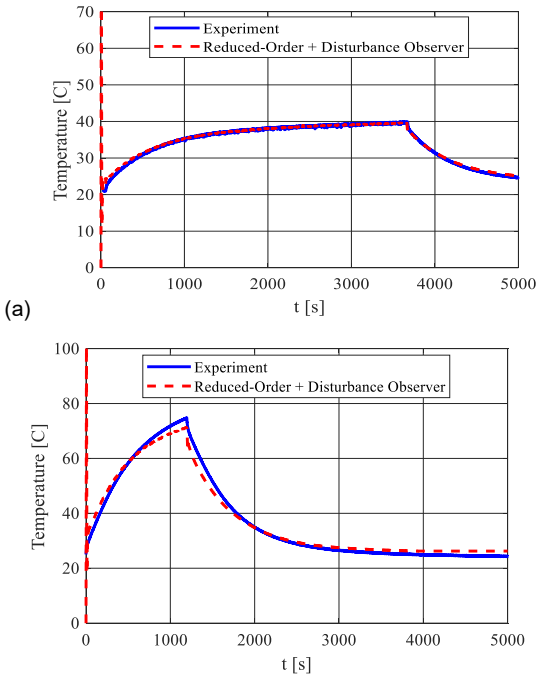

Fig 14.Comparison with Experimental Module. (a) 50A Peak Current; (b) 90A Peak Current;

It can be seen in Fig 14 that the transient thermal response of the observer model with disturbance estimation can match the experimental data both on heating step and cooling step, if ambient temperature is available. It is worth noting that despite the fact that the model placement and channel layout differ from those in the first experiment, both of the analytical models are supplied with the same set of parameters from the parameter estimation in Section III. From this, it can be concluded that the parameters related to the module geometry are of substantial importance, whereas parameters pertaining to the converter layout have only a negligible effect on the model. This knowledge can be used to reduce the amount of calculation required when determining these parameters considerably.

I. Conclusion

In this paper, a reduced order observer model with disturbance estimation is presented. The parameters used in the state-space matrices are obtained from a transient CFD model. By considering different experimental configurations it is demonstrated that these changes have relatively little impact on the parameters if the geometry of the power module remains the same. Therefore, once the power module design is fixed, changes to the number of modules and their relative layout do not influence the parameter estimation results, reducing the calculation load.

The inclusion of a disturbance observer in this model is important as it allows the model to adjust for errors caused by errors in the power losses estimation and inaccuracy in parameters estimation and uncertainties in the environmental and operating conditions. It is also worth noting that the air

temperature is a much simpler value to measure than the power dissipation, making it a more suitable input for the disturbance observer. The resulting model is shown to exhibit good accuracy and tracking capability, even under complex transient conditions, showing good correlation with the results obtained from a range of experimental tests. The method is computationally simple and therefore suitable for real-time application in industrial applications.

APPENDIX

Equations (1) and (2) can be derived by inspection from the thermal network in Fig. 2, where $X_{1,\dots,4}$ are the temperature rises across the respective capacitances.

$$C_1\frac{dX_1}{dt}+\frac{X_1}{R_1}=P_{loss}-\frac{X_1+X_2+X_3-X_4}{R_{jB}}$$

Then the above equation can be rewritten as

$$\frac{dX_1}{dt}=-\frac{1}{C_1}\left(\frac{1}{R_1}+\frac{1}{R_{jB}}\right)X_1-\frac{1}{C_1}\frac{X_2}{R_{jB}}-\frac{1}{C_1}\frac{X_3}{R_{jB}}+\frac{1}{C_1}\frac{X_4}{R_{jB}}+P_{loss}$$

Similarly

$$\frac{dX_2}{dt}=-\frac{1}{C_2}\frac{X_1}{R_{jB}}-\frac{1}{C_2}\left(-\left(\frac{1}{R_2}+\frac{1}{R_{jB}}\right)X_2\right)-\frac{1}{C_2}\frac{X_3}{R_{jB}}+\frac{1}{C_2}\frac{X_4}{R_{jB}}+P_{loss}$$

$$\frac{dX_3}{dt}=-\frac{1}{C_3}\frac{X_1}{R_{jB}}-\frac{1}{C_3}\frac{X_2}{R_{jB}}-\frac{1}{C_3}\left(-\left(\frac{1}{R_3}+\frac{1}{R_{jB}}\right)X_3\right)+\frac{1}{C_3}\frac{X_4}{R_{jB}}+P_{loss}$$

$$\frac{dX_4}{dt}=\frac{1}{C_4}\frac{X_1}{R_{jB}}+\frac{1}{C_4}\frac{X_2}{R_{jB}}+\frac{1}{C_4}\frac{X_3}{R_{jB}}-\frac{1}{C_4}\left(-\left(\frac{1}{R_4}+\frac{1}{R_{jB}}\right)X_4\right)$$

With simple reordering, the above equations can then be put into state-space formulation in equations (1) and (2). The parameters of the Foster network are:

Estimated Parameters					
R_1	1.71	R_2	3.59	R_3	2.40
R_4	11.27	R_{jB}	3.33	C_1	37.41
C_2	1.17	C_3	22.39	C_4	4.10

ACKNOWLEDGMENT

The Authors would like to thank Siemens AG Corporate Technology and Mr Oliver Raab in particular, for providing the power modules and data used in this research.

REFERENCES

[1] H. Wang, M. Liserre, and F. Blaabjerg, "Toward reliable power electronics: Challenges, design tools, and opportunities," *IEEE Ind. Electron. Mag.,* vol. 7, no. 2, pp. 17–26, 2013.

[2] A. Testa, S. De Caro, and S. Russo, "A Reliability Model for Power MOSFETs Working in Avalanche Mode Based on an Experimental Temperature Distribution Analysis," *IEEE Trans. Power Electron.*, vol. 27, no. 6, pp. 3093–3100, 2012.

[3] S. Yang, A. Bryant, P. Mawby, D. Xiang, L. Ran, and P. Tavner, "An industry-based survey of reliability in power electronic converters," *IEEE Trans. Ind. Appl.*, vol. 47, no. 3, pp. 1441–1451, 2011.

[4] A. T. Bryant, P. A. Mawby, P. R. Palmer, E. Santi, and J. L. Hudgins, "Exploration of Power Device Reliability using Compact Device Models and Fast Electro-Thermal Simulation," *Conf. Rec. 2006 IEEE Ind. Appl. Conf. Forty-First IAS Annu. Meet.*, vol. 3, no. c, pp. 1465–1472, 2006.

[5] H. Wang, K. Ma, and F. Blaabjerg, "Design for reliability of power electronic systems," *IECON 2012 - 38th Annu. Conf. IEEE Ind. Electron. Soc.*, pp. 33–44, 2012.

[6] M. Gerber, J. A. Ferreira, N. Seliger, and I. W. Hofsajer, "Integral 3-D thermal, electrical and mechanical design of an automotive DC/DC converter," *IEEE Trans. Power Electron*., vol. 20, no. 3, pp. 566–575, 2005.

[7] V. Smet et al., "Ageing and failure modes of IGBT modules in high-temperature power cycling," *IEEE Trans. Ind. Electron.*, vol. 58, no. 10, pp. 4931–4941, 2011.

[8] T. Herrmann, M. Feller, J. Lutz, R. Bayerer, and T. Licht, "Power cycling induced failure mechanisms in solder layers," *European Conference on Power Electronics and Applications*, Sept 2007.

[9] M. Andresen, K. Ma, G. Buticchi, J. Falck, F. Blaabjerg, and M. Liserre, "Junction Temperature Control for More Reliable Power Electronics," *IEEE Trans. Power Electron.*, vol. 33, no. 1, pp. 765–776, 2018.

[10] M. Musallam, C. M. Johnson, C. Yin, H. Lu, and C. Bailey, "In-service life consumption estimation in power modules," *2008 13th Int. Power Electron. Motion Control Conf. EPE-PEMC 2008*, pp. 76–83, 2008.

[11] Akbarzadeh, V., Levesque, J.-C., Gagne, C., & Parizeau, M. (2014). "Efficient sensor placement optimization using gradient descent and probabilistic coverage." Sensors, 14(8), 15525–15552.

[12] Z. Gao, C. Cecati and S. X. Ding, "A Survey of Fault Diagnosis and Fault-Tolerant Techniques—Part I: Fault Diagnosis With Model-Based and Signal-Based Approaches," in *IEEE Transactions on Industrial Electronics*, vol. 62, no. 6, pp. 3757-3767, June 2015. doi: 10.1109/TIE.2015.2417501.

[13] M. Musallam, C. Buttay, M. Whitehead, C. M. Johnson, and C. Buttay, "Real-Time Compact Electronic Thermal Modelling for Health Monitoring ", 1*2th European Conference on Power Electronics and Applications*, 2007.

[14] J. N. Davidson, D. A. Stone, M. P. Foster and D. T. Gladwin, "Real-Time Temperature Estimation in a Multiple Device Power Electronics System Subject to Dynamic Cooling," in *IEEE Transactions on Power Electronics*, vol. 31, no. 4, pp. 2709-2719, April 2016. doi: 10.1109/TPEL.2015.2443034.

[15] PJ Tannous, SRT Peddada, JT Allison, T Foulkes, RCN Pilawa-Podgurski, Andrew G Alleyne, "Model-based temperature estimation of power electronics systems", *Control Engineering Practice* 85, 206-215, April 2019.

[16] M. Iachello et al., "Lumped Parameter Modeling for Thermal Characterization of High-Power Modules," in *IEEE Transactions on Components, Packaging and Manufacturing Technology*, vol. 4, no. 10, pp. 1613-1623, Oct. 2014. doi: 10.1109/TCPMT.2014.2353695.

[17] J. Biela et al, "Impact of Power Density Maximization on Efficiency of DC–DC Converter Systems," *IEEE Trans. Power Electron*, vol. 24, no. 1, pp. 288-300, Jan. 2009.

[18] Y. Lei et al., "A 2-kW Single-Phase Seven-Level Flying Capacitor Multilevel Inverter With an Active Energy Buffer," *IEEE Trans. Power Electron*, vol. 32, no. 11, pp. 8570-8581, Nov. 2017.

[19] M. A. Eleffendi and C. M. Johnson, "Application of Kalman Filter to Estimate Junction Temperature in IGBT Power Modules," *IEEE Trans. Power Electron*., vol. 31, no. 2, pp. 1576–1587, 2016.

[20] A. Castellazzi, W. J. Choy, and P. Zanchetta, "Dynamic active cooling for improved power system reliability," *Microelectron. Reliab*., vol. 51, no. 9–11, pp. 1964–1967, 2011.

[21] X. Wang, A. Castellazzi, and P. Zanchetta, "Regulated Cooling for Reduced Thermal Cycling of Power Devices," *Proc. 7th Int. Power Electron. Motion Control Conf.*, vol. 1, pp. 238–244, 2012.

[22] M. Andresen, M. Schloh, G. Buticchi, and M. Liserre, "Computational light junction temperature estimator for active thermal control," in *Proc. IEEE Energy Convers. Congr. Expo*., 2016, pp. 1–7.

[23] X. Wang, A. Castellazzi, and P. Zanchetta, "Full-order observer based IGBT temperature online estimation," *IECON Proc. Industrial Electron. Conf.*, pp. 1494–1498, 2014.

[24] X. Wang, A. Castellazzi, and P. Zanchetta, "Observer based dynamic adaptive cooling system for power modules," *Microelectron. Reliab*., vol. 58, pp. 113–118, 2016.

[25] X. Wang, A. Castellazzi, and P. Zanchetta, "Temperature control for reduced thermal cycling of power devices," *15th Eur. Conf. Power Electron. Appl.*, pp. 1–10, 2013.

[26] C.H. can der Broeck, R.D. Lorenz, R. De Doncker, "Monitoring 3-D temperature distributions and device losses in power electronic

modules", *IEEE Trans. Power Electronics*, vol. 34, n. 8, Aug. 2019, pp. 7983-7995.

[27] M. Warwel, G. Wittler, M. Hirsch, and H. C. Reuss, "Real-time thermal monitoring of power semiconductors in power electronics using linear parameter-varying models for variable coolant flow situations," in *Proc. IEEE 15th Workshop Control Model. Power Electron*., Jun. 2014, pp. 1–6.

[28] M. Guacci, D. Bortis, I.F. Kovacevic-Badstuner, U. Grossner, J.W. Kolar, "Analysis and Design of a 1200 V All-SiC Planar Interconnection Power Module for Next Generation More Electrical Aircraft Power Electronic Building Blocks", *CPSS Trans. On Power Electronics and Appl.* Vol. 2, n.4, pp. 320-330, Dec. 2017

[29] K. Weidner, M. Kaspar, and N. Seliger, "Planar interconnect technology for power module system integration," in *Proc. of the 7th International Conference on Integrated Power Electronic Systems (CIPS)*, Nuremberg, Germany, 2012.

[30] www.i2mpect.eu

[31] F. Casanellas, "Losses in PWM inverters using IGBTs", *IEEE Proc. Electric Power Appl.*, vol. 141, n.5, pp. 235-239, Sep. 1994.

[32] T. Kamel, A. Griffo, J. Wang, "Modelling framework for parallel SiC power MOSFETs chips in modules developed by planar technology", *IEEE Int. Conf. on Electrical Systems for Aircraft, Railway, Ship Propulsion and Road Vehicles & International Transportation Electrification Conference (ESARS-ITEC)*, Nov. 2018.

[33] V. Sundarapandian, "Reduced order observer design for nonlinear systems," *Applied Mathematics Letters*, vol. 19, pp. 936–941, 2006.

[34] M. Darouach, M. Zasadzinski, and M. Hayar, "Reduced-order observer design for descriptor systems with unknown inputs", *IEEE Transaction on Automatic Control*, vol. 41, pp. 1068-1072, 1996.

[35] M. Darouach, M. Zasadzinski, and S.J. Xu, "Full-order observers for linear systems with unknown inputs", *IEEE Trans. Autom. Control*, 39, (3), pp. 606–609, 1994.

[36] M. Hou and P.C. Muller, "Design of observer for linear systems with unknown inputs", *IEEE Transaction on Automatic Control*, vol. 37, pp. 871-875 1992.

[37] Hui, S., Zak, S.H.: 'Observer design for systems with unknown inputs', *Int. J. Appl. Math. Comput. Sci*., pp. 431–446, 2005.

[38] K. Wang, A. N. Michel, and D. Liu, "Necessary and sufficient conditions for the Hurwitz and Schur stability of interval matrices," *IEEE Trans. Automat. Contr*., vol. 39, pp. 1251–1255, June 1994.

[39] E. Kaszkurewicz and A. Bhaya, *Matrix Diagonal Stability in Systems and Computation*. Boston, MA: Birkhäuser, 2000

[40] J. Rohn, "Positive definiteness and stability of interval matrices," *SIAM J. Matrix Anal. Appl*., vol. 15, pp. 175-184, 1994.

[41] www.opsens-solutions.com

[42] T. E. Salem, D. Ibitayo, and B. R. Geil, "Validation of Infrared Camera Thermal Measurements on High-Voltage Power Electronic Components", *IEEE Transactions on Instrumentation and Measurement*, Vol. 56, No. 5, Oct. 2007, pp. 1973-1978..

Xiaojun Dong received the B.Eng. degree in hydraulics and hydropower engineering from Northwest A&G University, Yangling, China, in 2014, and the M.Sc. degree in electronics and electrical engineering from University of Sheffield, Sheffield, U.K., in 2015. He is currently working toward the Ph.D. degree in electronics and electrical engineering at The University of Sheffield.
His current research focuses on thermal analysis of power electronics system.

Antonio Griffo (M'12) received the M.Sc. degree in electronic engineering and the Ph.D. degree in electrical engineering from the University of Napoli "Federico II," Naples, Italy, in 2003 and 2007, respectively. From 2007 to 2013, he was a Research Associate with The University of Sheffield, Sheffield, U.K., and the University of Bristol, Bristol, U.K. He is currently a Senior Lecturer in the Department of Electronic and Electrical Engineering, The University of Sheffield. His research interests include modeling, control, and condition monitoring of electric power systems, power electronics converters, and electrical motor drives for renewable energy, automotive, and aerospace applications..

David Hewitt received the MEng degree in Digital Electronics in 2011 and the PhD in Power Electronics in 2016 from the University of Sheffield, UK. He is currently a Research Associate at the University of Sheffield in the department of Electronic and Electrical Engineering working in the area of machine winding heath prognostics and winding fault detection methods. His research interests include reliability and prognostics, thermal modelling and passive components.

Jiabin Wang (SM'03) received the B.Eng. and M.Eng. degrees from Jiangsu University, Zhenjiang, China, in 1982 and 1986, respectively, and the Ph.D. degree from the University of East London, London, U.K., in 1996, all in electrical and electronic engineering. He is currently a Professor of electrical engineering at The University of Sheffield, Sheffield, U.K. From 1986 to 1991, he was with the Department of Electrical Engineering, Jiangsu University, where he was appointed a Lecturer in 1987 and an Associate Professor in 1990. He was a Postdoctoral Research Associate at The University of Sheffield from 1996 to 1997 and a Senior Lecturer at the University of East London from 1998 to 2001. His research interests range from motion control and electromechanical energy conversion to electric drives for applications in automotive, renewable energy, household appliances, and aerospace sectors.
Dr. Wang is a Fellow of the Institution of Engineering and Technology, U.K